High Stokes number wave focusing by a circular ridge: Internal, inertial and inertia–gravity waves

Natalia Shmakova, Jan-Bert Flór, Bruno Voisin, Joel Sommeria and Samuel Viboud

Laboratoire des Écoulements Géophysiques et Industriels (LEGI),
CNRS–Université Grenoble Alpes, F38000, Grenoble, France,
natalia.shmakova@legi.cnrs.fr

Abstract

We consider the focusing and breaking of internal waves generated by the horizontal oscillations of a very large torus mounted at the Coriolis platform, of 13 m diameter. The platform was filled with a linearly stratified fluid and rotated at a constant speed, or stood still to investigate, respectively, inertia–gravity or internal gravity waves. The wave field was measured using 2D or 3D PIV. The large torus size gives access to large Stokes numbers. Nonlinear effects and turbulence are observed in the focal region, but they can be described by linear theory with an eddy viscosity. Spectrum analysis shows the generation of higher harmonics in the focal zone even at low oscillation amplitude. The vertical vorticity field of internal gravity waves exhibits a dipolar structure in the focal zone, which transforms in the rotating case into a "Yin–Yang-shaped" structure. The overall structure of the inertial waves is close to that of internal gravity waves, though the overturning motion in the focal region is relatively intense.

1 Introduction

The generation of internal waves by oscillating objects is a long-standing subject of research in fluid mechanics and has its main applications in the Earth's oceans and atmosphere. In particular, in relation to ocean mixing, internal tides and their overturning have received considerable recent interest (Morozov, 1995; Garrett and Kunze, 2007). Internal tides are believed to transport energy through the ocean interior, and their breaking to cause energy dissipation estimated to be 1 TW .

In the laboratory, generally, waves are generated by two-dimensional objects such as cylinders and ridges, or three-dimensional objects such as spheres and ellipsoids. These are all simply connected objects. We consider a doubly connected object, the torus, which opens up a new possibility: wave focusing, to be considered as a possible scenario for energy concentration in localized zones representing hot spots for incipient overturning in the oceans. Different types of wave focusing exist, for instance when waves reflect on a boundary, in attractors or near density interfaces. Spontaneous geometric focusing may occur for forcing with a specific geometry, like a torus (Bühler and Muller, 2007; Grisouard and Bühler, 2012). Important mixing of stratification due to internal wave focusing of this latter type has been observed by Buijsman et al. (2014) in Luzon Strait, and may be a cause for the mixing observed by Peliz et al. (2009) at Tore seamount.

First experiments on geometric focusing have been conducted by Duran-Matute et al. (2013) who obtained wave turbulence in the focal region for a vertically oscillating torus in a rotating fluid. Ermanyuk et al. (2016) showed with a horizontally oscillating torus in a linearly stratified fluid that at low Stokes numbers $St \approx 200$ the wave amplitude increases toward the focal region, forming one zone of amplitude amplification. In this zone one expects overturning and mixing of waves.
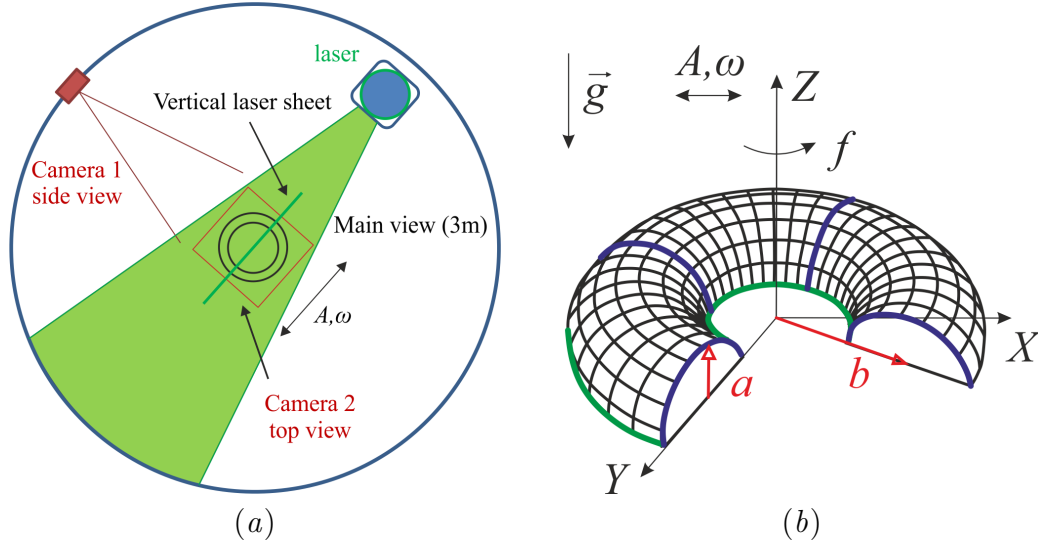
Figure 1: (*a*) Top view of the experimental setup at the Coriolis platform; (*b*) geometry of the torus with parameters and notations.

The present experimental results were obtained for a much larger torus of minor radius $a = 15$ cm and major radius $b = 75$ cm, giving access to large Stokes number $St \approx 4500$. They report some new aspects of the dynamics of internal focusing waves in rotating and stratified fluids, and the possibility of wave breaking in the focal region.

2   Experimental setup

Experiments were conducted at the Coriolis platform, a cylindrical tank 13 m in diameter and 1 m of working depth (figure 1*a*). The platform, which either stood still or rotated, was filled with water linearly stratified in density by salinity to a depth $H = 90$ cm. The stratification was measured with two conductivity probes, moving up and down by a computer-controlled motor. The buoyancy frequency was kept constant for experiments in the stratified fluid at $N = \left(-\frac{g}{\rho}\frac{d\rho}{dz}\right)^{1/2} = 0.5$ rad/s, where $\rho(z)$ is the density profile along the vertical axis, and g is the gravity. In the rotating case the inertial frequency was fixed at $f = 0.2$ rad/s.

In all experiments, waves were generated by the horizontal oscillations of a torus of minor radius $a = 15$ cm and major radius $b = 75$ cm. The oscillations had frequency ω and amplitude A. The torus, made of plexiglas, was cut in half horizontally and fitted upside down on a plexiglas plate kept at the surface of the fluid (see figure 1*b*). A Cartesian coordinate system is introduced with origin at the centre of the torus, x and y-axes parallel and normal to the direction of oscillations, respectively, and z-axis normal to the free surface. The coordinates X, Y and Z are normalized with the minor radius a.

Waves were visualized with Particle Image Velocimetry (PIV) (Westerweel, 1997) and Volume PIV techniques. For that the fluid was seeded with polystyrene particles of 200 μm in the stratified case, and with Orgasol® 60 μm particles in the rotating case. For a standard PIV measurement the particles were visualised with a vertical laser sheet in the centre plane parallel to the direction of oscillation ($Y = 0$). Images were taken with a 12-bit Dalsa camera of CCD 1024×1024 px. The visualisation of volumes was performed

with a horizontal laser sheet moving vertically up and down and the motion of the laser sheet was controlled by a motor. Images in volumes were taken by a Falcon high speed camera with resolution 2432×1728 px.

3   Results

Internal waves are generated according to the dispersion relation

$$\omega = \sqrt{f^2 \sin^2 \theta + N^2 \cos^2 \theta}, \qquad (1)$$

with θ the angle between the wave beam and the vertical. Depending on whether the fluid is stratified and still ($N \neq 0, f = 0$), or stratified and rotating ($N \neq 0, f \neq 0$), or homogeneous and rotating ($N = 0, f \neq 0$), we shall refer to the waves as internal gravity, inertia–gravity or inertial, respectively. In the present experiments we consider the angle θ to be fixed ($\approx 60°$) for all types of waves for better comparison. In the case of internal gravity waves this angle corresponds to $\omega/N = \arccos\theta = 0.51$, so that all harmonics but the first are evanescent (Mowbray and Rarity, 1967). Measurements are performed at a nondimensional oscillation amplitude $A/a = 0.17$ for all experiments, which is as close as possible given the setup to the tidal oscillation amplitude in the real ocean.

3.1   Vorticity field

The difference between the internal waves generated in stratified and/or rotating fluid is studied by considering the horizontal and vertical vorticity fields. In the presence of rotation (figure 2b), inertia–gravity wave motion is found over a bigger region than for internal gravity waves. This is because the waves propagate in beams, with edges at the critical rays tangent to the torus and to its image at the surface. For inertia–gravity waves, these rays turn out to be further apart than for internal gravity waves. The reason for this is unclear, but seems connected with the boundary layer at the mounting plate supporting the torus, since this is where reflection takes place. As a consequence, there are four clearly identifiable separate zones of critical ray intersection in figure 2 (b), compared with one single diamond-shaped zone of intersection of wave beams in figure 2 (a). The vertical vorticity field of internal gravity waves exhibits a dipolar structure in the focal zone, which transforms for inertia–gravity waves into a "Yin–Yang-shaped" structure (figure 2d,e). The overall structure of the inertial wave beams (figure 2c) resembles that for internal gravity waves. The overturning motion in the focal region is intense, and results there in a vertically standing inertial wave motion with alternating red-blue vorticity (McEwan, 1973).

The three-dimensional view of the vertical vorticity field was reconstructed from the Volume PIV measurements, and its isosurfaces are presented in figures 3 (a) and (b) for internal gravity and inertia–gravity waves, respectively. The presence of a dipolar vortex for the nonrotating stratified fluid demonstrates nonlinear effects in the focal zone of internal gravity waves (figure 3a). The vorticity structure for inertia–gravity waves reveals that the positive and negative vortices are twisted around each other (figure 3b). This motion takes place through 2/3 of the depth. The Rossby radius of deformation was calculated as $R = (Nh)/f$, with $h = 2H/3$, and predicts the size of the vortex to be 150 cm, close to what has been observed.
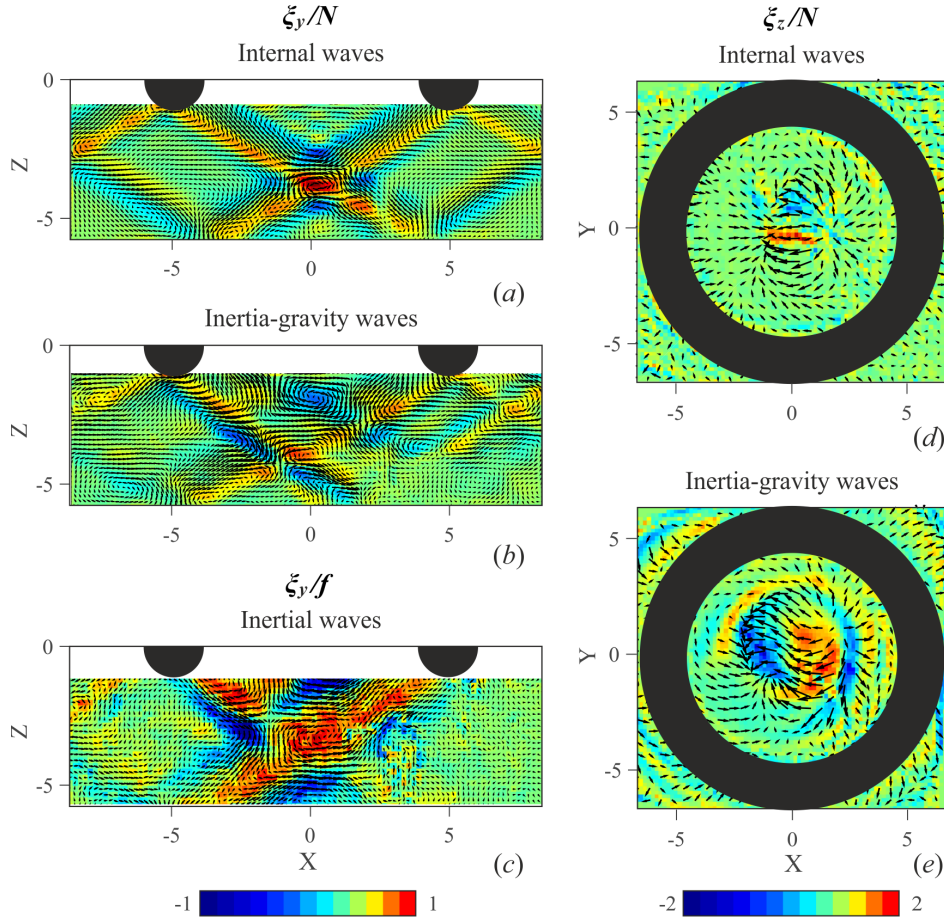
Figure 2: Instantaneous velocity vectors together with (a-c) instantaneous horizontal transverse vorticity, ξ_y/N or ξ_y/f, in the vertical plane of oscillation $Y = 0$ (the color scale is the same in all three images), and (d,e) vertical vorticity, ξ_z/N, in the horizontal plane through the centre $Z = -4$ of the focal zone for internal gravity waves (the color scale is the same in both images).
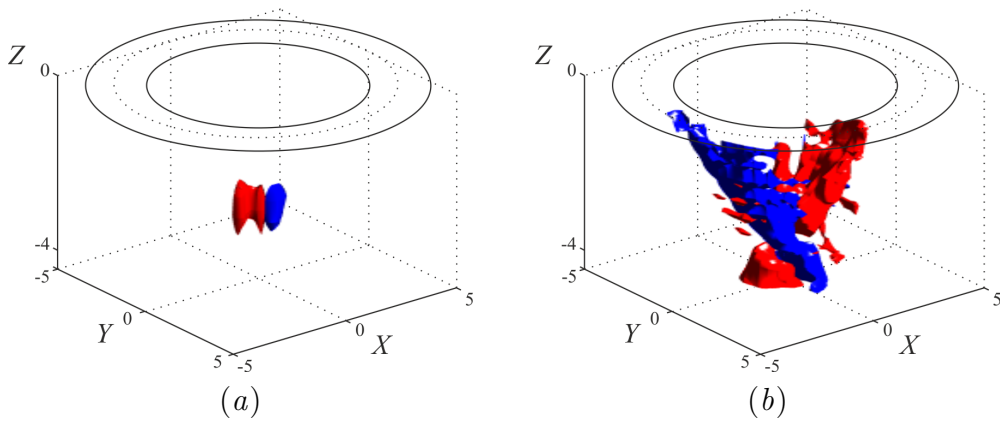

Figure 3: Isosurface of the instantaneous vertical vorticity field $\xi_z/N = \pm 0.6$, reconstructed from the volume PIV measurements for (a) internal gravity waves and (b) inertia–gravity waves. Red and blue colors indicate positive and negative vorticities, respectively. The horizontal section of the torus at $Z = 0$ is shown with black curves.
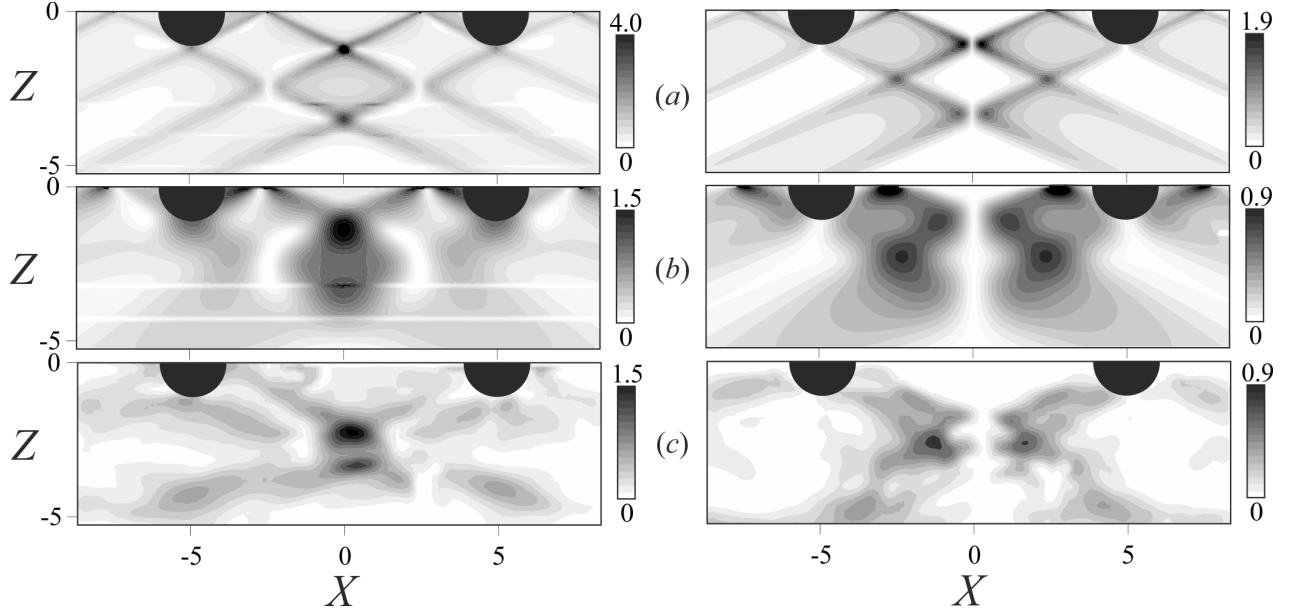
Figure 4: Horizontal velocity amplitude U_1 (left column) and vertical velocity amplitude W_1 (right column) internal gravity waves in the vertical plane of symmetry $Y = 0$: (a) theoretical predictions based on molecular viscosity; (b) theoretical predictions based on eddy viscosity $\nu = 0.4$ m^2/s; (c) experimental results after filtering the first harmonic. The occurrence of spurious maxima at $Z = 0$ in the theory is discussed in Voisin (2016).

3.2 Comparison with the linear theory

The linear theory described in Voisin (2016) allows us to calculate the amplitude of internal gravity waves which may be expected for high Stokes number $St = (\omega a^2)/\nu = 4500$, with $\nu = 0.01$ cm^2/s the molecular viscosity. These results are presented in figure 4 (a) for the horizontal longitudinal U_1 and vertical W_1 velocity components in the vertical plane $Y = 0$, and show the bimodal structure of the wave beams. Comparing this with experimental results in figure 4 (c), one notices a difference in structure. This difference can be caused by mixing in the turbulent boundary layer at the surface of the torus. Theoretical formulas can be therefore recalculated with an eddy viscosity $\nu_{eddy} = 0.4$ cm^2/s $\gg \nu$. These results are presented in figure 4 (b) and show better agreement with the experiment in figure 4 (c). The focal zone is formed of two zones of amplitude amplification in the centre for the horizontal velocity and four zones of amplitude amplification for the vertical velocity. Another specificity of the experimental wave beams is the origin of generation. The upper critical ray delimiting the wave beam is vertically shifted downwards compared with the theoretical calculations, and with the experimental and numerical observations for a hemisphere (King et al., 2009). As a consequence, the upper part of the focal zone is lower than predicted. This shift is caused by the turbulent motion close to the surface of the fluid and to the mounting plate. However the lower part of the focal region is well predicted by the linear theory calculated with eddy viscosity ν_{eddy} (see figure 4b and c at $Z = -3$ for the horizontal longitudinal velocity and $Z = -2.5$ for the vertical velocity).

The internal gravity and inertia–gravity waves are compared in terms of the vertical distribution of the horizontally averaged total kinetic energy. Amplification is observed in the focal zone in the stratified case, and also close to the surface in the rotating stratified case (figure 5a).
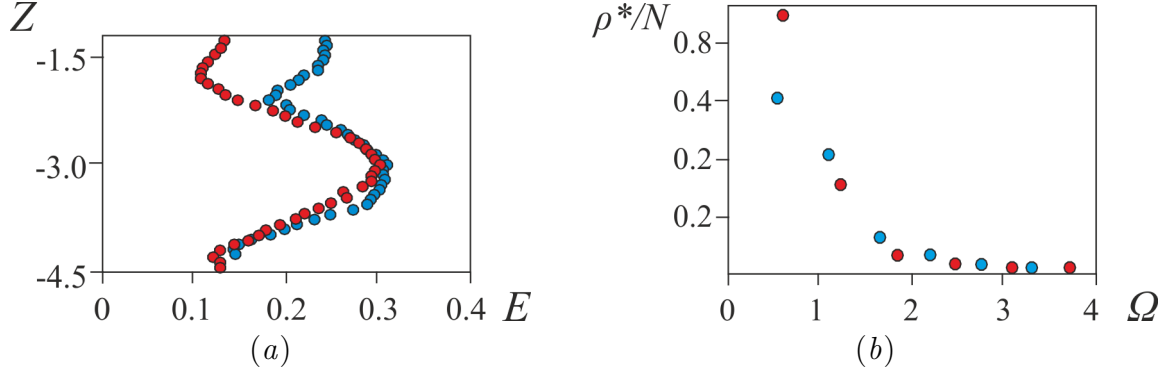
Figure 5: (a) Vertical distribution of total kinetic energy averaged along the horizontal; (b) Fourier-filtered density amplitude ρ^* against normalized oscillation frequency, $\Omega = \omega/N$, based on conductivity data from the probe in the focal zone. Blue and red dots represent results for internal gravity and inertia–gravity waves, respectively.

3.3 Time-frequency representation

The time–frequency representation (see e.g. Flandrin, 1999) is performed for the horizontal longitudinal velocity u:

$$S(t,\omega) = \left\langle \left| \int_{-\infty}^{+\infty} du \; u \exp^{-i\omega u} h(t-u) \right|^2 \right\rangle_{xy} , \qquad (2)$$

where $h(t) = 0.54 - 0.46\cos(\omega t)$ is a Hamming window. Figures 6 (a) and (b) show the result averaged over a small area close to the torus and in the focal zone, respectively. Close to the torus the first two harmonics of internal gravity waves appear. In the focal zone the nonlinear interactions result even for low oscillation amplitude $A/a = 0.17$ in the generation of evanescent higher harmonics after four oscillation periods. From the experimental results we notice that with the present sizes of the object and experimental tank nonlinear effects always take place in the focal region, by contrast with the observations at lower sizes by Ermanyuk et al. (2016). Fourier filtering of the density signal obtained with a conductivity probe in the focal zone (figure 5b) shows that the density amplitude normalised with the buoyancy frequency, ρ^*/N, has a maximum at the fundamental frequency and decreases nearly exponentially with increasing harmonic frequency $n\omega/N$ for internal gravity as well as for inertia–gravity waves. This result is in agreement with that obtained from the velocity field (figure 6b) which also shows qualitatively a decrease in energy with increasing frequency $n\Omega$. Therefore, the energy distribution is similar for internal gravity and inertia–gravity waves.

4   Conclusions

We have measured the 3D wave structure for internal gravity, inertial and inertia–gravity waves. The horizontal vorticity field has a similar structure for internal gravity and inertial waves, though the intensity of the motion is higher for inertial waves and the vorticity spreads through the entire depth due to energy loss by diapycnal mixing. In the case of both rotation and stratification four vortices have been observed in the focal region. The vorticity field demonstrates the presence of nonlinear effects in the focal zone which cause dipolar motion. For inertia–gravity waves this motion is twisted and spreads through
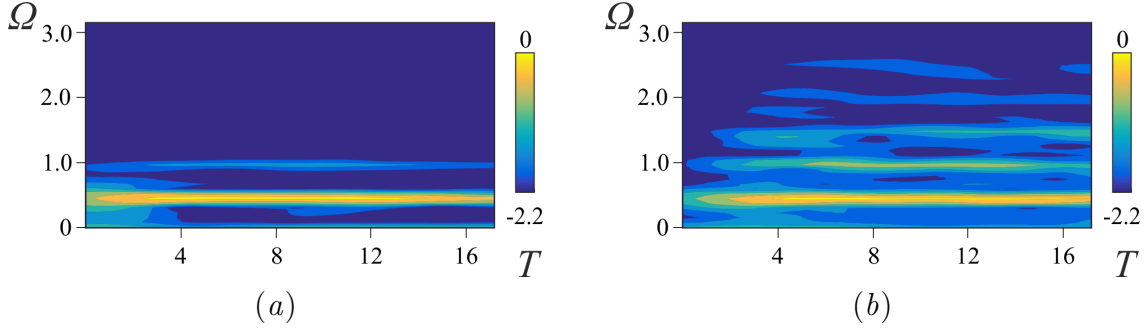
Figure 6: Time–frequency diagram of $\log_{10}(S_U(t,\omega)/S(t,\omega_0))$ for internal gravity waves. The horizontal velocity u is averaged over areas (a) $-5 < X < -4$, $Y = 0$, $-1.7 < Z < -1$ (near field) and (b) $-1 < X < 1$, $Y = 0$, $-4 < Z < -2.6$ (focal zone). The experimental parameters are $N = 0.5$ rad/s, $\omega/N = 0.51$, $A/a = 0.17$ and the normalized variables are $\Omega = \omega/N$ and $T = (\omega t)/2\pi$.

2/3 of the fluid depth. The size of the vortex is well predicted by the Rossby radius of deformation.

Spectral analysis of the velocity and density in the focal zone shows the generation of higher harmonics due to wave beam interaction. Most of the energy is in the fundamental wave, whereas the higher harmonics are evanescent and their energy decreases exponentially.

Our large scale experiment, providing Stokes number of 4500, generates turbulence in the focal region, a source of mean flow generation and mixing. The effect of this turbulence on the wave beam can be taken into account by means of an eddy viscosity.

Acknowledgements

References

Bühler, O. and Muller, C. (2007). Instability and focusing of internal tides in the deep ocean. *J. Fluid Mech.*, 588:1–28.

Buijsman, M., Klymak, J., Legg, S., Alford, M., Farmer, D., MacKinnon, J., Nash, J., Park, J.-H., Pickering, A., and Simmons, H. (2014). Three-dimensional double-ridge internal tide resonance in Luzon strait. *J. Phys. Oceanogr.*, 44:850–869.

Duran-Matute, M., Flór, J.-B., Godeferd, F. S., and Jause-Labert, C. (2013). Turbulence and columnar vortex formation through inertial-wave focusing. *Phys. Rev. E*, 87:041001(R).

Ermanyuk, E., Shmakova, N., and Flór, J.-B. (2016). Internal wave focusing by a horizontally oscillating torus. *accepted for J. Fluid Mech.*

Flandrin, P. (1999). *Time–Frequency/Time–Scale Analysis*. Academic Press, San Diego.

Garrett, C. and Kunze, E. (2007). Internal tide generation in the deep ocean. *Annu. Rev. Fluid Mech.*, 39:57–87.

Grisouard, N. and Bühler, O. (2012). Forcing of oceanic mean flows by dissipating internal tides. *J. Fluid Mech.*, 708:250–278.

King, B., Zhang, H. P., and Swinney, H. L. (2009). Tidal flow over three-dimensional topography in a stratified fluid. *Phys. Fluids*, 21:116601.

McEwan, A. D. (1973). A laboratory demonstration of angular momentum mixing. *Geophys. Fluid Dyn.*, 5:283–311.

Morozov, E. G. (1995). Semidiurnal internal wave global field. *Deep-Sea Res I*, 42:135–148.

Mowbray, D. E. and Rarity, B. S. H. (1967). A theoretical and experimental investigation of the phase configuration of internal waves of small amplitude in a density stratified liquid. *J. Fluid Mech.*, 28:1–16.

Peliz, A., Le Cann, B., and Mohn, C. (2009). Circulation and mixing in a deep submerged crater: Tore seamount. *Geophysical Research Abstracts*, 11:EGU2009–7567.

Voisin, B. (2016). Internal wave focusing by annular forcing. *This conference.*

Westerweel, J. (1997). Fundamentals of digital particle image velocimetry. *Measurement Science and Technology*, 8:1379–1392.